IEEE Transactions on Nuclear Science, Vol.NS-22, No.3, June 1975

COMPARISON OF STANDING WAVE ACCELERATORS OPERATING IN THE $2\pi/3$ AND $\pi/2$ MODES

S.O. Schriber

Atomic Energy of Canada Limited
Chalk River Nuclear Laboratories
Chalk River, Ontario, Canada

Summary

Calculations of fields in standing wave accelerators operating in the $2\pi/3$ and $\pi/2$ modes have been done using a set of RLC coupled loop circuits to determine equilibrium current solutions. These results have been compared to experimental on-axis field measurements in an S-band accelerating structure. Tolerances of the two systems to frequency and coupling-constant differences are discussed as well as to operation slightly off-resonance. All results indicate that the $\pi/2$ mode is significantly less sensitive to construction and operational differences.

Introduction

Advantages in using the $\pi/2$-mode as a standing-wave acceleration mode for a coupled-cavity linear accelerator are stability of the cavity fields with respect to frequency differences cell-to-cell, cavity losses and beam loading[1]. The mode is stable because every second cell has minimal excitation. Other modes have been proposed and used for standing-wave linacs, in particular the $2\pi/3$-mode[2,3]. Again, this mode is stable because every third cell has minimal excitation[4].

A linear accelerator employing on-axis couplers would favor operation in the $2\pi/3$-mode (triperiodic) over the $\pi/2$-mode (biperiodic) if the only criterion was the number of on-axis couplers - the number of couplers is halved. The $2\pi/3$-mode system could also have a 2.5% higher effective shunt impedance if pancake couplers[5] were used. However, a comparison of the relative stabilities of the two modes is necessary to determine which is best for a particular application. This paper reports calculations and measurements which show why the $\pi/2$-mode should be the preferred mode when stability requirements override advantages of fewer coupling cells.

Calculations

A set of coupled rf resonators has been represented by a coupled-loop equivalent circuit consisting of R,L,C elements as previously described[6]. A similar model was used here except that one loop included an rf voltage generator to drive the system. Relative axial electric field amplitudes for the physical system were represented by the loop-current solutions of the coupled equations. Computer solutions of the complex equations, as a function of rf frequency at constant drive voltage, gave complex loop-current values with associated loop phases relative to the rf generator at 0°. The resonance criterion for the appropriate mode was that there be a maximum in the drive loop current amplitude. The computer program could consider different frequencies and quality factors for each loop of the equivalent circuit. Also, each coupling constant (rf coupling between cells was represented by the mutual inductance between loops) could be made different. Thus solutions of the equations could be made to represent a given physical system if the corresponding values for each cell (of the system) were known.

Experimental System

The singly periodic (all cells identical) 23 cell system used for experimental measurements of relative axial electric field amplitudes had the following mean parameters;

f (individual resonant frequency)	- 2988.52 MHz
Q (individual cell quality factor)	- 7500
k (first neighbour coupling constant)	- 3.15%

The system shown schematically in Figure 1 employed off-axis coupling slots and LALA[7]-shaped half cavities. Successive segments were oriented 90° to each other to eliminate second neighbour couplings. Individual cell frequencies were within an 0.5 MHz band. Cell frequency changes were made by adjusting a small copper collar inserted in the segment beam hole. Collar movement into the cavity field volume lowered the cell frequency. Individual cell frequencies were measured prior to assembly for on-axis field measurements. The component segments were clamped in a horizontal press resulting in coupled mode quality factors of 7500.

Standard bead pull techniques were used to determine on-axis electric field amplitudes. The resonant frequency of the chosen mode as a function of the axial position of a 2 mm dielectric bead was plotted on an x-y recorder. Resonance was maintained by an automatic frequency control (AFC) circuit employing phase sensitive detectors and an fm-modulated rf signal generator. Rf drive to the coupled system and rf pick-up for the feedback AFC circuit were by magnetic loops in the first cell. Analysis of the results considered;

a) the possibility of field amplitude errors due to the bead being off-axis in the cells - found to be negligible.

b) the change in the axial distribution of the detuned cell because of the tuning collar.

c) end cell differences due to the termination, and

d) effects of the drive and pick-up loops in the first cell.

Comparison of Model Calculations with Experiment

Measurements of the 23 mode frequencies and quality factors, and the relative peak heights mode-to-mode for a constant rf drive were in excellent agreement with the equivalent-circuit model calculations. A more stringent test of the model is the comparison of cell field levels with and without component differences. Some typical comparative results are given below, all with the rf drive at cell 1. Excellent agreement was noted between calculations and measurements of relative axial electric field amplitudes for both the $\pi/2$ and $2\pi/3$ mode.

Calculated and measured relative axial electric field amplitudes (normalized at cell 5) for the $\pi/2$ mode are shown in Figure 2 with cell 13 detuned -12.7 MHz. Notice the reasonable agreement and that the "accelerating" cell amplitudes vary by at most ± 3.2% (calculated). Figures 3 and 4 present similar results (calculations and measurements normalized at cell 4) for the $2\pi/3$ mode with cells 13 (Figure 3) and 11 (Figure 4) detuned by -12.7 MHz. Again notice the reasonable agreement between calculations and measurements for all cells - "coupling" and "accelerating". Although the "coupling" cells exhibit similar properties, the $2\pi/3$-mode has "accelerating" cell amplitude variations ± 24.1% (calculated) which are eight times larger than the $\pi/2$-mode variations. This amplitude variation has two components, one for each of the adjacent "accelerating" cells. For ease of discussion with the $2\pi/3$-mode, cells numbered $3\ell-2$ and $3\ell-1$ will be known as "cross" and "dot" cells respectively where $\ell=1, 2, 3 \ldots$ Figures 3 and 4 show that if a "cross" or "dot" cell is perturbed in frequency, it is the opposite type group of cells which exhibits the largest amplitude variation.

Measured and calculated results were in agreement for detuning any "coupling" cell -12.7 MHz and showed that the relative field amplitudes were insensitive to coupler detuning for either mode as expected.

A further test of the model is shown in Figures 5 and 6 where both end cells were detuned +5.7 MHz and the third cell for the $\pi/2$ mode (fourth cell for the $2\pi/3$ mode) was detuned -12.7 MHz. There is good agreement between calculations and measurements for both modes. Fluctuations in cell amplitude are larger in the $2\pi/3$-mode than in the $\pi/2$ mode.

Comparisons of Other $2\pi/3$ and $\pi/2$ Mode Calculations

The agreement of the model with observation was considered adequate to justify the model's use in comparing other properties of the two modes without further recourse to experiment. Calculations discussed in the following examples were based on a 29 cell (20 accelerating cells, 9 couplers) $2\pi/3$-mode (triperiodic - see Figure 1) system and a 41 cell (21 accelerating cells, 20 couplers) $\pi/2$-mode (biperiodic - see Figure 1) system with full cell terminations, f = 3000 MHz and k = 4%. All cells have the same quality factor and the two systems have approximately the same number of accelerating cells.

a) Random Frequency Errors

Table 1 gives results of phase and amplitude calculations for the two systems. Cell frequency errors were generated by a random number generator routine having a flat distribution over a frequency range, a possible situation when cells are selected within an "acceptance tolerance". Several results given for each frequency tolerance limit are for different sets of generated random frequencies - to ensure that a proper perspective is obtained and no chance distortion occurs. The relative phase indicates the maximum variation in phase relative to zero at the drive cell. The $\pi/2$-mode is clearly not as sensitive to frequency errors as the $2\pi/3$-mode by at least an order of magnitude. The "0" frequency limit shows a systematic tilt from the drive cell due to the finite Q. In the $\pi/2$-mode, frequency errors up to ±2 times the cell bandwidth do no more than introduce phase shifts whereas in the $2\pi/3$-mode such changes result in significant amplitude variations.

b) Coupling Constants

$\pi/2$-mode calculations for a coupling-constant difference of "a"% between coupler ℓ and accelerating cell $\ell-1$ or $\ell+1$, with the drive at cell N ($N > \ell$), resulted in field amplitudes in accelerating cells one to $\ell-1$ differing from the rest by "a"%, as expected. Relative phases were unaffected. A similar situation for the $2\pi/3$-mode is shown in Figure 7 where accelerating cells are labelled by either "crosses" or "dots". The three different results for a "cross" drive cell are as follows where the amplitude difference is equal to the coupling constant ratio:

1) Coupling difference between a "dot" cell and coupler - Field amplitudes in every "dot" cell between the drive cell and the bad coupled cell differ from the drive cell value.

2) Coupling difference between adjacent accelerating cells - Field amplitudes in every "dot" cell between the drive cell and the bad coupled pair differ from the drive cell.

3) Coupling difference between a "cross" cell and coupler - Field amplitudes in every "dot" cell between the drive cell and the bad coupled cell differ from the drive cell value and amplitudes in every "dot" and "cross" cell outside of these bounds differ from the drive cell value.

With the $\pi/2$ mode, the location of a coupling constant fault can be relatively easy to determine because of the abrupt change in field amplitude. This is not so with the $2\pi/3$ mode because field amplitude changes can be reflected throughout the full length of the coupled system. The $2\pi/3$ mode situation becomes much more complicated for more than one system coupling fault.

c) End Cells

For the first and last cell detuned +10 MHz and -10 MHz respectively, the change in $2\pi/3$-mode amplitudes is shown in Figure 8; the associated maximum phase shift being 4.5°. Very large differences occur between the neighbouring accelerating cells. A similar detuning for the $\pi/2$ mode operation results in field amplitudes remaining within 0.08% with an associated maximum phase shift of 1.2°.

Tuning the end half cells of the last cells in these coupled systems must be done correctly. This is difficult because these cells do not have the symmetry (i.e. no coupling slots) of the other cells. This example shows that the sensitivity to this tuning step is much greater for the $2\pi/3$-mode than the $\pi/2$ mode.

d) Systematic Frequency Error

Figure 9 shows the effect of a systematic frequency error from cell-to-cell for the two modes, in this case a cosine error distribution from end-to-end as illustrated. Again the $2\pi/3$-mode is much more sensitive and shows the two component nature of the fields.

e) Off Resonance Characteristics

Figure 10 shows the results of driving the $\pi/2$ and $2\pi/3$ modes off-resonance. The range in relative "accelerating" cell axial electric field amplitudes is shown as a function of frequency with the drive cell normalized to unity. The resonance curve should be used to determine the absolute values relative to the on-resonance amplitude of unity - the drive cell axial field amplitude is reduced by $\sqrt{2}$ and $\sqrt{5}$ relative to the on-resonance amplitudes when the driving frequency is off-resonance by Δf and $2\Delta f$ respectively ($\Delta f = f/2Q$). In both modes, coupling cell amplitudes relative to their on-resonance values remain the same over this narrow frequency range. Since the coupler amplitudes do not increase and since they are less than 5% of the on-resonance axial accelerating cell amplitudes, an accelerator could be operated at different accelerating gradients by driving off-resonance. Figure 10 shows that the $2\pi/3$ mode has much larger excursions in accelerating cell field amplitudes than the $\pi/2$ mode for off-resonance operation.

Conclusions

The loop-coupled R,L,C equivalent circuit model yields results which agree well with experimental measurements on the effects of errors in singly periodic coupled resonator systems. Not only was there agreement between the different mode frequencies and relative excitation intensities, but agreement with individual cell field amplitudes has been shown.

The model (supported by some experimental results) shows that the $\pi/2$ mode is a better standing wave linear accelerator operating mode than the $2\pi/3$ one because it is markedly less sensitive to perturbations.

Because in a real system the "coupling" cells are made very short (in fact ring or side couplers result in structures of identical length) it is not immediately evident without examining the particular application whether cost savings from halving the number of couplers will be more than offset by costs from considerably tightened tolerances.

References

1. Knapp E.A., Knapp B.C., and Potter J.M., Rev. Sci. Instr. 39, 979, 1968.

2. Epsztein B. and Tran D.T., Proc. of 1968 Proton Linac Conf., BNL 50120, 457, 1968.

3. Bensussan A., Tran D.T., and Tronc D., Nucl. Instr. and Meth., 118, 349, 1974.

4. Swenson D.A., Knapp E.A. and Swain G.R., Proc. of 1969 Part. Accel. Conf., IEEE Trans. Nucl. Sci., NS-16, 338, 1969.

5. Schriber S.O., Heighway E.A. and Funk L.W., Proc. of 1972 Proton Linac Conf., LA-5115, 140, 1972.

6. Schriber S.O., Proc. of 1972 Proton Linac Conf., LA-5115, 407, 1972.

7. Hoyt H.C., Simmons D.D. and Rich W.F., Rev. Sci. Instr. 37, 755, 1966.

Table 1: Relative Field and Phase Variation for $\pi/2$ and $2\pi/3$ Modes

Quality Factor	Frequency Tolerance Limits	$\pi/2$ MODE		$2\pi/3$ MODE	
		Relative Field Amplitudes	Phase Relative to the Drive Cell	Relative Field Amplitudes	Phase Relative to the Drive Cell
11,000	0 kHz	0.08%	0°	0.09%	4.1°
11,000	± 500 kHz	0.08% 0.07% 0.09% 0.06%	0.06° 0.16° 0.10° 0.04°	4.8% 4.0% 3.4% 3.4% 3.6% 3.8%	4° 4° 4° 4° 4° 4°
5,500	0 kHz	0.3%	0°	0.35%	8.1°
5,500	± 500 kHz	0.3% 0.29% 0.32% 0.3%	0.13° 0.34° 0.22° 0.09°	4.8% 4.1% 4.4% 3.4% 3.4% 5.9%	8.0° 8.0° 8.1° 8.1° 8.2° 8.1°

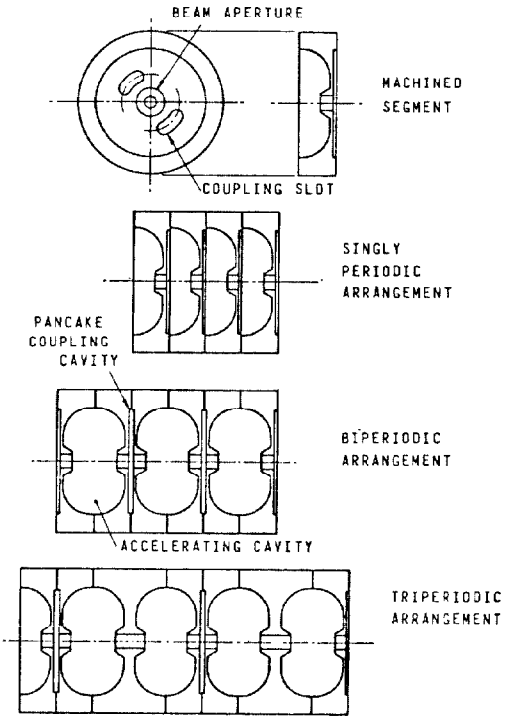

Figure 1: Schematic sectional arrangement of single periodic, biperiodic and triperiodic systems with a cross-sectional view of a component segment.

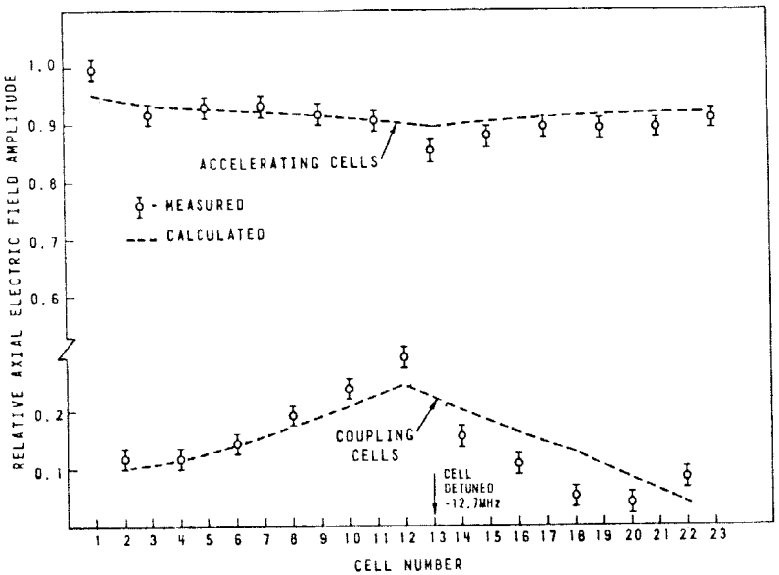

Figure 2: Comparison of measured and calculated $\pi/2$-mode axial electric field amplitudes for cell 13 detuned -12.7 MHz.

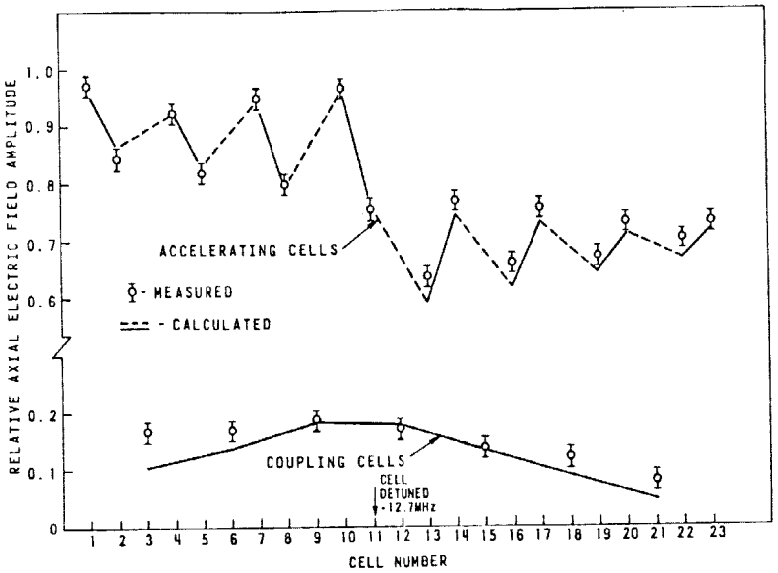

Figure 4: Comparison of measured and calculated $2\pi/3$-mode axial electric field amplitudes for cell 11 detuned -12.7 MHz (the solid line for the accelerating cell amplitudes connects adjacent accelerating cells).

Figure 3: Comparison of measured and calculated $2\pi/3$-mode axial electric field amplitudes for cell 13 detuned -12.7 MHz (the solid line for the accelerating cell amplitudes connects adjacent accelerating cells).

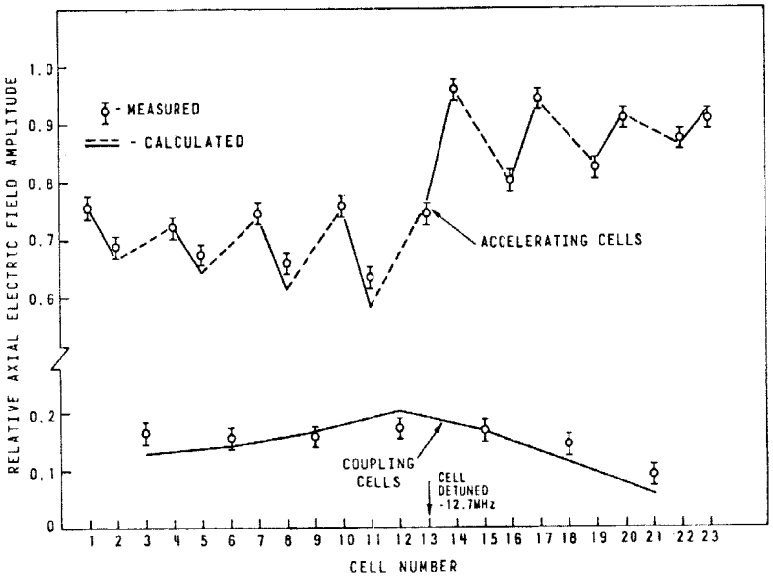

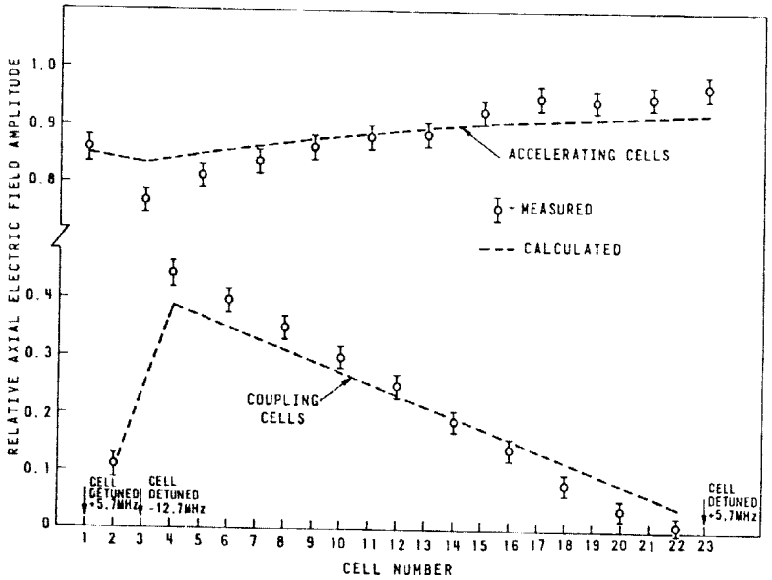

Figure 5: Comparison of measured and calculated $\pi/2$-mode axial electric field amplitudes for cell 3 detuned -12.7 MHz and the end cells detuned +5.7 MHz.

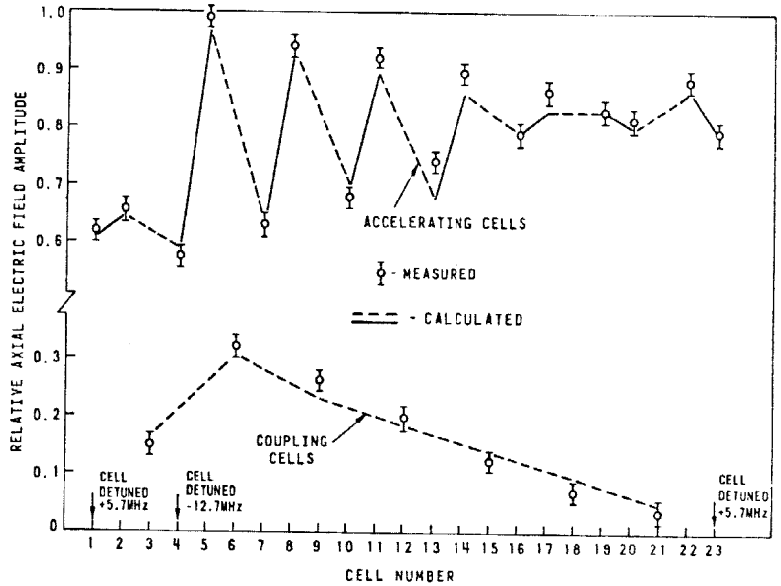

Figure 6: Comparison of measured and calculated $2\pi/3$-mode axial electric field amplitudes for cell 4 detuned -12.7 MHz and the end cells detuned +5.7 MHz (the solid line for the accelerating cell amplitudes connects adjacent accelerating cells).

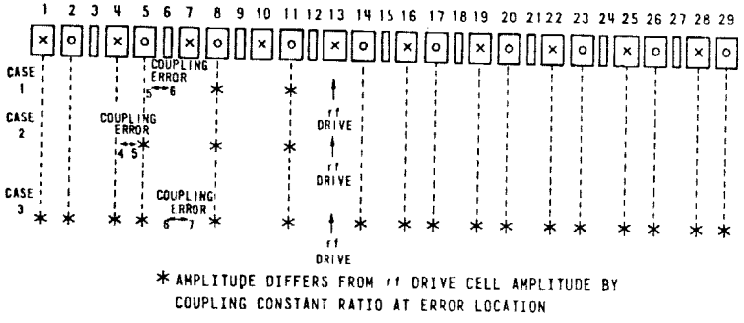

Figure 7: Three cases of $2\pi/3$-mode field amplitudes with coupling-constant errors between cells 5 and 6, cells 4 and 5 and cells 6 and 7. "x" and "o" (cross and dot) cells are accelerating cells as identified in the text, unlabelled cells are couplers.

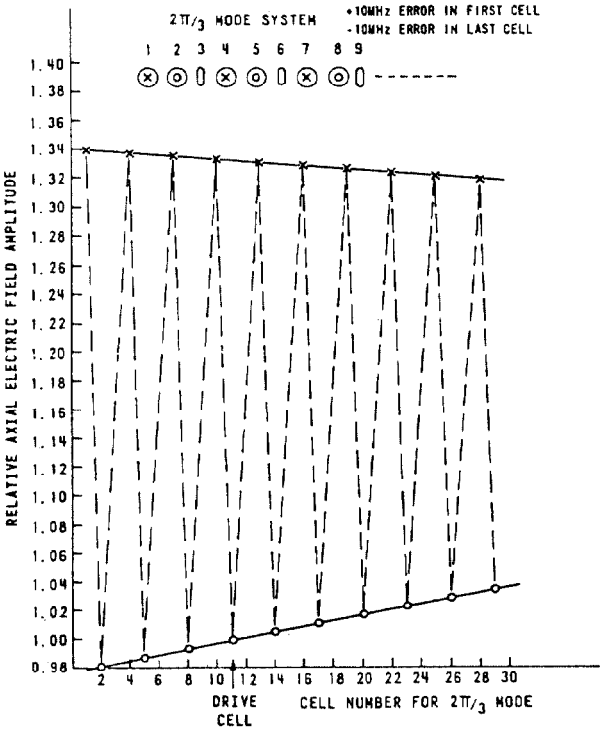

Figure 8: Calculated $2\pi/3$-mode axial electric field amplitudes for the first cell detuned +10 MHz and the last cell detuned -10 MHz.

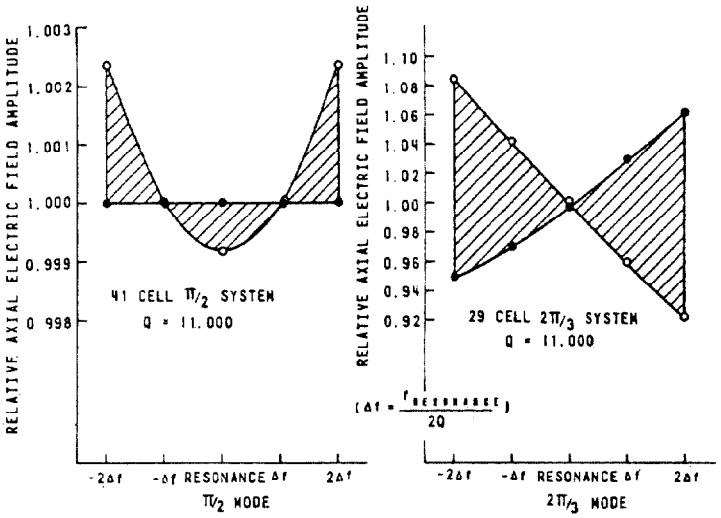

Figure 10: Range of relative axial electric field variations cell-to-cell for the $\pi/2$ and $2\pi/3$ modes as a function of frequency with the drive cell normalized to unity.

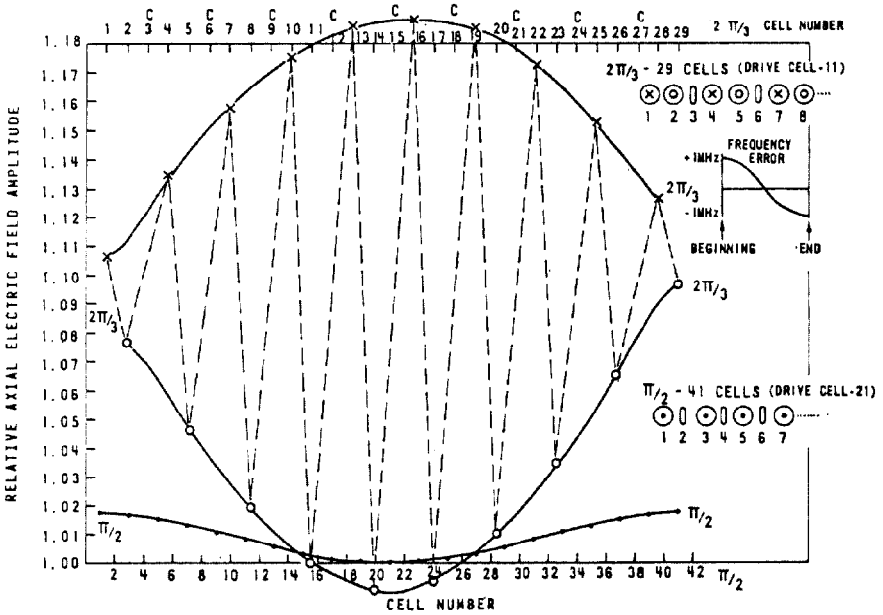

Figure 9: Calculated $2\pi/3$-mode axial electric field amplitude for a systematic frequency error represented by a cosine distribution of 1 MHz amplitude (coupling cells for the $2\pi/3$-mode are signified by C).